Synthesis, antibacterial evaluation, crystal structure determination, hirshfeld surface analysis and density functional theory analysis of novel 3-amino-2-(2-thienyl)-4(3H)-quinazolinone

Mohammed Geesi, Yassine Riadi, Abdellah Kaiba, Talal Aljohani, Philippe Guionneau

Synthesis, Antibacterial Evaluation, Crystal Structure Determination, Hirshfeld Surface Analysis and Density Functional Theory Analysis of Novel 3-Amino-2-(2-Thienyl)-4(3H)-Quinazolinone

Mohammed H. Geesi[1*], Yassine Riadi[2], Abdellah Kaiba[3], Talal Aljohani[4], Philippe Guionneau[5]

[1]Department of Chemistry, College of science and humanities in Al-Kharj, Prince Sattam bin Abdulaziz University, Al-Kharj 11942, Saudi Arabia.
[2]Department of Pharmaceutical Chemistry, College of Pharmacy, Prince Sattam bin Abdulaziz University, Al-Kharj 11942, Saudi Arabia.
[3]Department of physic, College of science and humanities in Al-Kharj, Prince Sattam bin Abdulaziz University, Al-Kharj 11942, Saudi Arabia.
[4]Department of Pharmaceutics, College of Pharmacy, Prince Sattam bin Abdulaziz University, Al-Kharj 11942, Saudi Arabia.
[5]CNRS, Univ. Bordeaux, Bordeaux INP, ICMCB, UMR 5026, 87 av. Dr A. Schweitzer, F-33600 Pessac (France).

∗ Corresponding author. Tel.: +966 5 374 931 75; e-mail: y.riadi@psau.edu.sa/yassinriadi@yahoo.fr

Abstract

A single crystal of new 2-substitued quinazoline derivative has been successfully synthesized through a simple and novel process based on a two-step reaction involving cyclisation, oxidation and hydrasination. The structure of the newly synthesized product was fully characterized by spectroscopic analysis NMR (^{1}H & ^{13}C), IR and HRMS. This intriguing compound crystalizes crystallises in a monoclinic system with P21/c space group. Notably, the stability of crystal packing was assured via hydrogen bonds, π- stacking and van der Waals interactions. An intermolecular interaction examination of the crystal structure was performed using Hirshfeld surface analysis and two-dimensional fingerprint plots. In addition, the electrostatic surface potential was calculated using density functional theory. In addition, the 3-amino-2-(2-thienyl)-4(3H)-quinazolinone, was applied to selected bacterial strains, and its antibacterial activity was assessed. In addition, a molecular docking study has been realised.

Keywords: Quinazoline, Antibacterial, Crystal structure, Hirshfeld surface analysis, Density functional theory

Introduction

Bacterial resistance stands as a prominent contributor to the escalating mortality rates attributed to infectious diseases in human populations [1-3]. This phenomenon is globally on the rise, primarily driven by the misapplication and excessive utilization of antimicrobial agents [4]. Estimates suggest an annual toll of approximately 700,000 deaths attributable to drug-resistant pathogens, a figure projected to surge to 10 million by 2050 if current trajectories persist [5]. Many human infections remain asymptomatic and latent, compounding the complexity of the situation, particularly with the emergence of bacterial strains resistant to single and combinational drug therapies [6]. Thus, there exists an urgent imperative for the development of novel and efficacious antibacterial agents to combat the prevailing menace of multidrug-resistant bacteria. One promising avenue involves the exploration of combination therapies featuring two or more pharmacophores or the synthesis of hybrid compounds incorporating multiple bioactive entities, offering potential solutions against multidrug-resistant bacterial strains [6]. A quinazoline core is a structural scaffold found in many natural products, such as lutonin, bouchardatine, 2-methylquinazolin-4(3H)-one and 2-(4-hydroxybutyl)quinazolin-4(3H)-one [7-10], as well as various pharmaceutical drugs, such as **gefitinib**, **erlotinib, Caneratinib** and **lapatinib** [11] (**Fig.1**). Quinazoline encompasses a family of heterocyclic compounds with a wide variety of pharmacological properties. For example, certain quinazoline derivatives have been shown to have strong anti-inflammatory [12], antibacterial [13], antifungal [14], antituberculosis [15], analgesic [16], antimalarial [17], antidiabetic [18], antipsychotic [19] and anticancer effects [20].

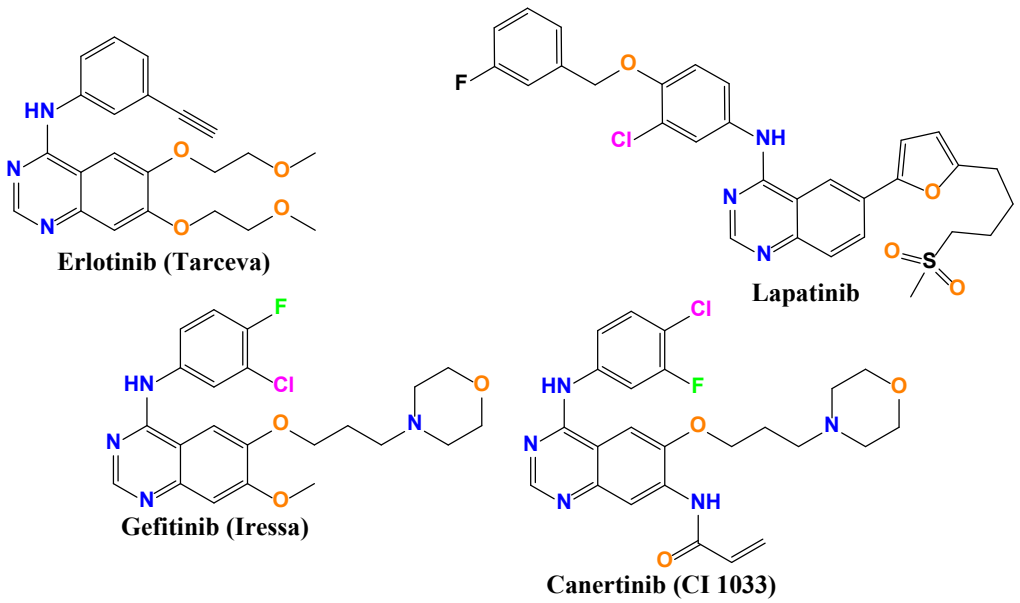

Fig 1. Chemical structure of certain quinazoline-based medications

Quinazoline scaffolds are one of the largest structural compounds to demonstrate potent inhibitory efficacy against epidermal growth factor receptor, which plays an important role in the generation of tumours [21]. Several methods have been employed to prepare quinazoline derivatives, including Aza–Diels–Alder reaction [22], Aza-Wittig reaction [23], microwave-assisted synthesis [24], metal-mediated

reaction [25-27], phase-transfer catalysis [28], ultrasound-mediated synthesis [29], oxidative cyclisation [30] and one-pot synthesis [31]. In view of previous rational and in continuation of our research for newer antibacterial agents. In the present study and according to the bibliographic data presented below, we have decided to synthesize a quinazoline derivative substituted at two positions, with a thiophene-type group attached to carbon atom C2 and an NH_2-type group attached to nitrogen atom N1. Additionally, we have replaced the N-aryl groups documented in the literature with a carbonyl group, and finally, eliminated all benzene substitutions from the quinazoline skeleton (**Fig. 2**). Also, the structure of the 3-Amino-2-(2-thienyl)-4(3H)-quinazolinone was confirmed using single-crystal X-ray diffraction analysis, and the derivative was applied to selected bacterial strains to test its antibacterial activity.

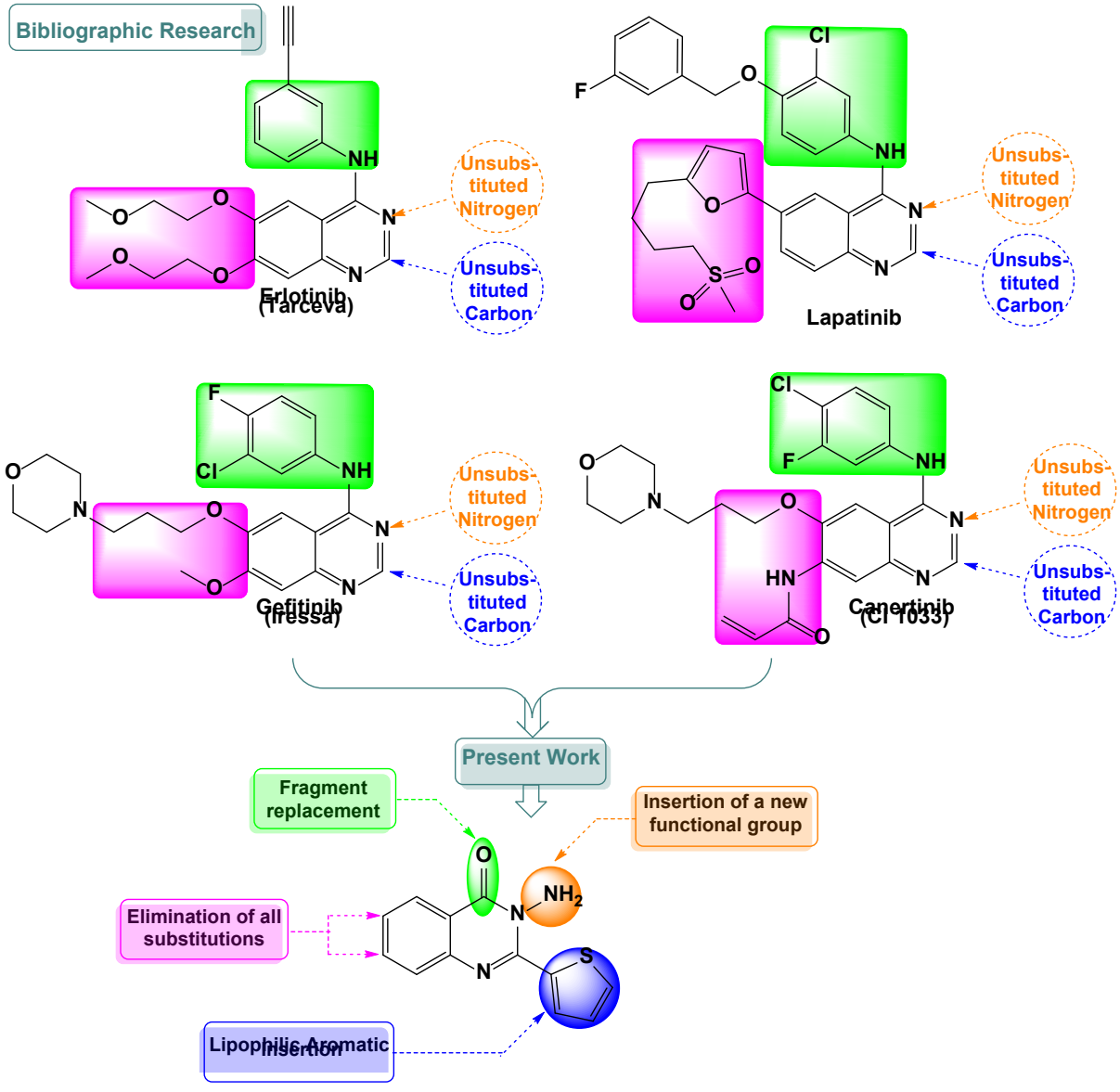

Fig.2. Molecular design of the target quinazoline derivative

Materials and methods

Chemistry

The reagents (chemicals), were purchased from commercial sources (Aldrich and Acros). The melting points (mp) of all the synthesized compounds were determined in capillary apparatus and are inaccurate. Analytical thin-layer chromatography (TLC) was performed on plates percolated with E. Merck silica gel 60 F254 to a thickness of 0.25 mm. IR spectra were recorded on a Bruker Vertex 70 spectro-photometer using potassium bromide discs in the frequency range 4000-400 cm^{-1}. HRMS were obtained on a Q-TOF micromass spectrometer. ^{1}H and ^{13}C NMR spectra were recorded in DMSO-d6 with 500 MHz Bruker Avance III spectrometer with a BBFO+ probe. Chemical shifts (δ) are expressed in parts per million (ppm) and coupling constants (J) are mentioned in Hz. It is worthy to mention here that compound **3** was isolated and identified according to the previously reported method [32].

General procedure for derivative 3-Amino-2-(2-thienyl)-4(3H)-quinazolinone 4.

3-Amino-2-(2-thienyl)-4(3H)-quinazolinone **4** was prepared according to the following method. To a solution of intermediate **3** in dried ethanol (10 mL), hydrazine (in excess) was added. The reaction mixture was heated under reflux with stirring for 1h. After completion of the reaction (the reaction was monitored by TLC), the solvent and and hydrazine were evaporated under reduced pressure. The crude product was collected, filtered and recrystallised from ethanol to produce the final product, 3-amino-2-(2-thienyl)-4(3H)-quinazolinone, with a yield of 79%.

3-Amino-2-(2-thienyl)-4(3H)-quinazolinone 4. White solid, 79%. mp = 128-130°C. ^{1}H NMR δ (ppm): 7.21-7.23 (1H, ddd, H-Ar); 7.46-7.50 (1H, ddd, H-Ar); 7.66-7.68 (1H, ddd, H-Ar); 7.78 -7.83 (1H, ddd, H-Ar); 7.86-7.87 (1H, dd, *J* = 8.0 Hz, H-Ar); 8.11-8.13 (1H, dd, 10.0 Hz, H-Ar); 8.42-8.41; (1H, d, *J* = 6.5 Hz, H-Ar). ^{13}C NMR δ (ppm): 119.71 (Cq); 126.53 (CH); 126.68 (CH); 127.41 (CH); 127.66 (CH); 134.33 (Cq); 134.48 (CH); 134.95 (CH); 135.49 (C=N); 147.24 (Cq); 150.08 (Cq); 161.73 (-C=O). FT-IR (KBr disk, υ_{max}, cm^{-1}): 496; 714; 762; 849; 951; 1241; 1333; 1464; 1528; 1665; 2257. HRMS (TOF-MS ES+) (m/z) $[M+H]^{+}$ calculated for $C_{12}H_9N_3OS$: 244.0501; found: 244.0515.

Structure solution and refinement

Data on single-crystal $C_{12}H_9N_3OS$ were collected using a Bruker Apex II diffractometer equipped with a molybdenum anticathode and graphite monochromator. All crystallographic and refinement data on this structure are summarised in **Table 1**. A structural hypothesis proposing a determination of the structure was supplied by the SIR97 programme [33]. The structure was performed using the SHELX97 programme, and a refinement was performed based on the full-matrix least-squares technique using the SHELXL programme [34]. The hydrogen atoms were theoretically determined. The MERCURY programme was used for structural visualisation [35]. All these programmes are part of program package

WinGX-Version 2023.1 [36]. All crystallographic data can be viewed for free online (www.ccdc.cam.ac.uk/data_request/cif).

Hirshfeld surface and 2D fingerprint plots

The Hirshfeld surfaces calculated for compound **4** provide additional information on the distinctive contributions made to molecular packing. Thus, a Hirshfeld surface analysis [37] and the associated two-dimensional fingerprint plots [38] were performed using CrystalExplorer17.5 [39] to figure out the normalized contact distance (dnorm), which depends on contact distances to the closest atoms outside (de) and inside (di) the surface. The molecular HS was performed using a standard (high) surface resolution with the three-dimensional surfaces mapped over a fixed color scale of -0.4586 to 1.4592a.u. The electrostatic potential was generated using TONTO implanted in Crystal Explorer 17.5 with the 6-31g(d,p) basis set at the Hartree–Fock level of theory, energy in the range -0.1010 to +0.1299 a.u.

Quantum chemical calculations

The quantum chemical calculation was done through DFT calculations using Gaussian 16w package version 6.1.1. All geometry optimization was performed employing the B3LYP/6-311+G(d, p) basis set [40] and all obtained frequencies are positive, proving that all structure corresponds to minimum energy. The implicit solvent effect was considered employing the integral equation formalism polarizable continuum model (CPCM) [41].

Antibacterial assay

In vitro antibacterial activity of the synthesized compound **4** was studied against four bacteria strains using broth microdilution technique. All equipment and culture media were sterilised before use. The bacteria tested comprised of Gram-positive bacterial strains methicillin-resistant Staphylococcus aureus (MRSA) and Bacillus cereus (Bc) and the gram-negative strains Klebsiella pneumoniae (Kp) and Escherichia coli (E. coli). DMSO was used as the negative control. The MIC was calculated as follows. First, concentrations of derivative **4** were set at 100, 75, 50, 38.5, 25, 18.75 and 12.5 µg/mL in the DMSO. Subsequently, 200 µL of the serially diluted test samples was dispensed into the 96-well microtrays. Next, bacterial samples were inoculated into the wells, with the final volume set to 400 µL. This was followed by incubation of the plates at 37°C for 24 h. The concentration through which a clear reduction in turbidity was observed was referred to as the MIC. All experiments were carried out in triplicate. Viable bacteria were confirmed in the presence of resazurin dye after 4 h of incubation, and the MIC was taken for each compound.

Physico-chemical Properties

The pharmacological action of any drug depends upon its physico-chemical properties. These properties include Log P (partition coefficient), TPSA (topological polar surface area), molecular weight (MW), hydrogen bond acceptors (HBA), hydrogen bond donors (HBD), number of rotatable bonds, and violations. The physico-chemical properties were calculated by using Molinspiration software [42]. Molinspiration offers a molecular processing and property calculation toolkit written in Java. Rule of 5 Properties is set of simple molecular descriptors used by Lipinski in formulating his "Rule of 5". The rule states, that most "drug-like" molecules have logP <= 5, molecular weight <= 500, number of hydrogen bond acceptors <= 10, and number of hydrogen bond donors <= 5. Molecules violating more than one of these rules may have problems with bioavailability [43].

Toxicity

Computational methodologies have greatly improved the ability to assess toxicity, delivering crucial safety insights for chemical compounds through in silico techniques. These methods enable the comprehensive evaluation of toxicity factors like Hepatotoxicity, Carcinogenicity, Immunotoxicity, and Mutagenicity. Utilizing the ProTox II server, which accepts compounds in SMILES format, facilitated the prediction of toxicity parameters for the designed compounds [44].

Molecular Docking

Molecular Docking was performed by using Auto dock 4.2 version. The selected ligand incorporated into UCSF Chimera by SMILES notation, and then converted into 3D structure further, subjected to energy minimization, resulting in PDB files. The selected proteins for molecular docking includes Klebsiella pneumoniae (PDB ID: 5O7N), E.Coli (PDB ID: 2JVU), Methicillin-resistant Staphylococcus aureus (PDB ID: 2W9S), and Bacillus cereus (PDB ID: 2HUC), were obtained from RCS Protein data bank in PDF format. The protein preparation, was processed by removing residues and water molecules. Polar hydrogens and Kollmann charges were added for valency balance. PDB files were converted to PDBQT files by accessing the torsions section and saving them accordingly. Grid box generation involved opening the macromolecule in the grid, setting dimensions at a 90-degree axis, saving the settings as .gpf file for grid parameter file generation. Docking procedures included selecting search and genetic parameters, opting for the Lamarckian genetic algorithm, and saving configurations as .dpf files for dock parameter file generation. Parameter files were converted to log files via command prompt, and the output was saved as a .dlg file. Analysis involved activating conformations and visualizing interactions between the enzyme and ligand. The obtained .dlg files were then analysed in BIOVIA Discovery Studio, where ligand-protein interactions were explored in both 2D and 3D format [45].

Results and discussion

Synthesis

Our method for synthesizing 3-amino-2-(2-thienyl)-4(3H)-quinazolinone **4** comprises two steps. Initially, anthranilic acid **1** underwent a transformation into 2-(thiophen-2-yl)-4H-benzo[d][1,3]oxazin-4-one **3** by combining it with 2-thiophenecarboxaldehyde **2**, facilitated by iodine and potassium permanganate in ethanol (10 mL) under microwave irradiation for 30 minutes. After allowing the mixture to cool to room temperature, it was poured into a saturated solution of $Na_2S_2O_3$ and then extracted with ethyl acetate followed by evaporation of the solvent. The resulting crude product was subjected to purification via column chromatography on silica gel, yielding intermediate **3** in an 86% yield. The compound **3** was subjected to a substitution reaction with hydrazine then brought to reflux for one hour. Thereafter, the crude product was collected, filtered and recrystallised from ethanol to produce the final product, 3-amino-2-(2-thienyl)-4(3H)-quinazolinone, with a yield of 79% (**Scheme 1**).

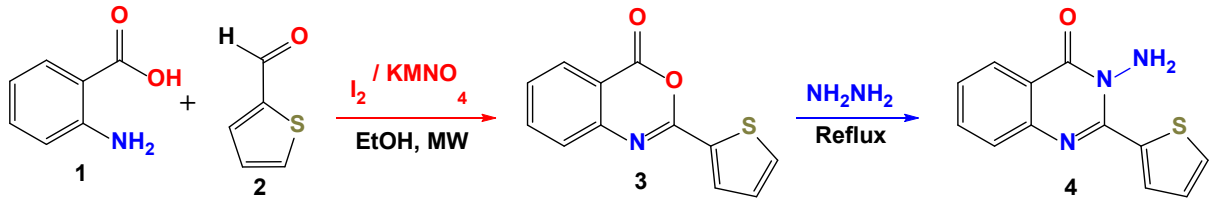

Scheme 1. Strategy of synthesis of targeted novel 3-Amino-2-(2-thienyl)-4(3H)-quinazolinone **4**

It should be pointed out that the NMR spectrum of the product **3** no shows resonances of -NH and -OH, this means that the two starting materials were hybridized. However, the FT-IR and NMR spectra of product **4** clearly show a signal characterizing the function amine ($-NH_2$) at (NMR: δ ^{1}H 3.75 ppm) and (FT-IR: υmax 1528 cm^{-1}). This means that the oxygen atom of compound **3** was substituted by the hydrazine. Furthermore, the ^{1}H NMR spectrum of the final product **4** also revealed the presence of Sp2 hybridized ethylenic protons. Among these protons, 3 originate from the thiophene nucleus and 4 protons from the aryl group, these protons are observed between 7.00 and 8.50 ppm. The ^{13}C NMR spectrum reveals two deshielded peaks at δ 161.73 and 147.24 ppm, attributable to the two carbons of the C=O and C=N groups, respectively. In addition, its HRMS spectrum shows the corresponding pseudo-molecular ion $[M+H]^+$ at m/z = 244.0515, consistent with the molecular formula $C_{12}H_9N_3OS$ proposed to the final product. In light of all these spectral evidences, we can confirm that the final product of our synthesis is stable under these operating conditions. Furthermore, the likely mechanism of the reaction between intermediate compound **3** and hydrazine is proposed in **Figure 3**. Initially, compound **3** is activated by hydrazine at the lactone function, forming a less stable intermediate **B**. This, through simple conjugation with the oxygen of the oxazine cycle, causes the opening of this cycle to yield compound **C**. Additionally, a tautomeric equilibrium followed by intramolecular cyclization leads to the formation of compound **C**.

Subsequently, during a water elimination reaction, compound **E** is transferred to produce the targeted compound **4**.

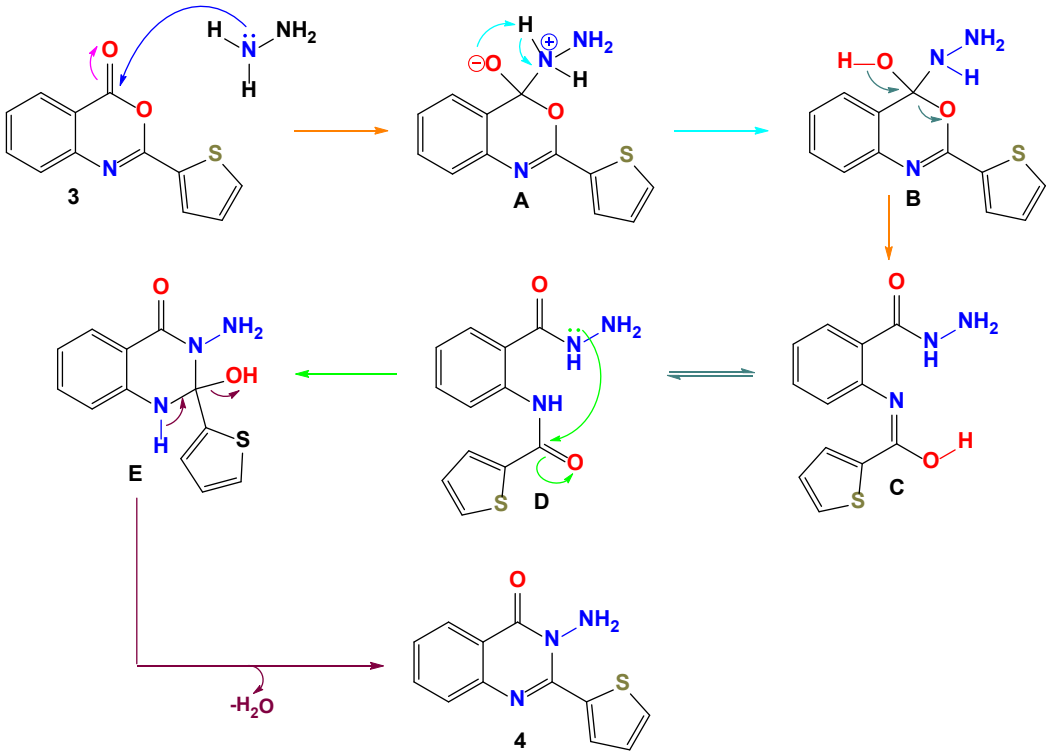

Fig.3. The proposed mechanism of the formation of quinazolinone **4**

Crystal structure description

Data on single-crystal $C_{12}H_9N_3OS$ were collected using a Bruker Apex II diffractometer equipped with a molybdenum anticathode and graphite monochromator. All crystallographic and refinement data on this structure are summarised in **Table 1**. All crystallographic data can be viewed for free online (www.ccdc.cam.ac.uk/data_request/cif).

Table 1. Crystallographic and structure refinement data

Empirical formula	$C_{12}H_9N_3OS$	
Formula weight	243.28	
Temperature	293 K	
Wavelength	0.71073 Å	
Crystal system	Monoclinic	
Space group	P 21/c	
Unit cell dimensions	a = 14.5361 Å	
	b = 4.62770 Å	β= 106.4°.
	c = 16.6899 Å	
Volume	1076.8 Å^3	
Z	4	

Density (calculated)	1.501 Mg/m^3
Absorption coefficient	0.285 mm^{-1}
F(000)	504
Theta range for data collection	2.5447 to 29.6020°.
Index ranges	-19<=h<=19, -6<=k<=6, -22<=l<=22
Reflections collected	20880
Independent reflections	2136 [R(int) = 0.0326]
Completeness to theta = 25.242°	99.9 %
Refinement method	Full-matrix least-squares on F^2
Data / restraints / parameters	2668 / 0 / 155
Goodness-of-fit on F^2	1.079
Final R indices [I>2sigma(I)]	R1 = 0.0463, wR2 = 0.1345
R indices (all data)	R1 = 0.0602, wR2 = 0.1220
Largest diff. peak and hole	0.480 and -0.214 $e.Å^{-3}$

The structure identified following the refinement showed that the compound crystallises in a monoclinic system, and specifically in the P21/c space group, with the following unit cell parameters: ***a*** = 14.5361(4) (4) Å, ***b*** = 4.6277(1) Å, ***c*** = 16.6899(5) Å, ***β*** = 106.4 (2) and ***Z*** = 4. The unit cell contains four $C_{12}H_9N_3OS$ molecules (**Figure 4b**).

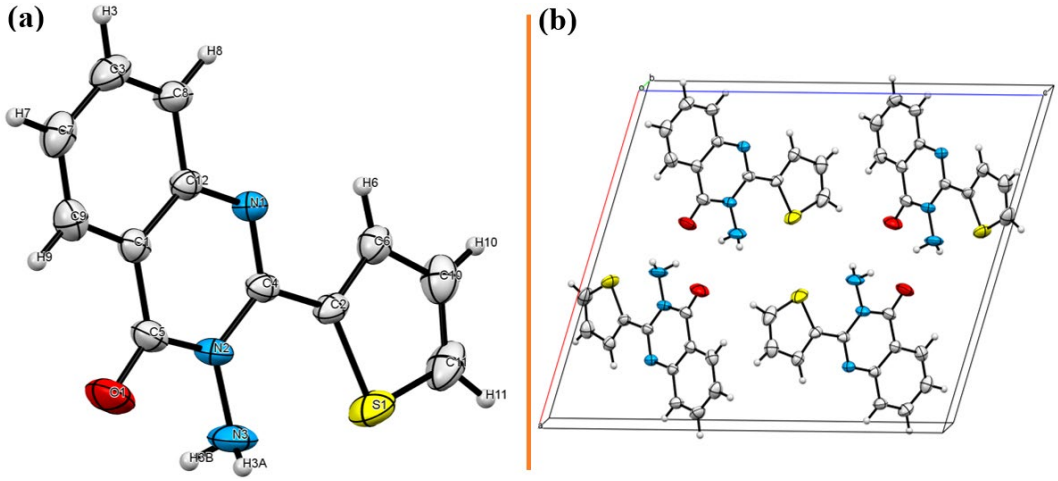

Fig.4. View along b axis of asymmetric unit (a) and the unit cell of the titled compound $C_{12}H_9N_3OS$ (b).

The crystal structure comprises a network of intermolecular hydrogen bonds and weak π-π stacking interactions (**Fig.5**). Each molecule coheres with five neighbouring molecules: there is an intramolecular hydrogen bond interaction between the sulphur atom of the 2-thienyl radical moiety and NH_2 (S…NH_2) across a distance of 2.729 Å; an intermolecular hydrogen bond interaction between the sulphur atoms of the 2-thienyl radical moiety (S….S) across a distance of 3.339 Å; two intermolecular hydrogen bond interactions (C=O…NH_2) across distances of 2.291 Å; and weak π- π stacking interactions between the

2-thienyl radical moiety and C_6H_4- ring via CH across distances of about 3.584 Å and 3.606 Å (**Fig.5**) [46].

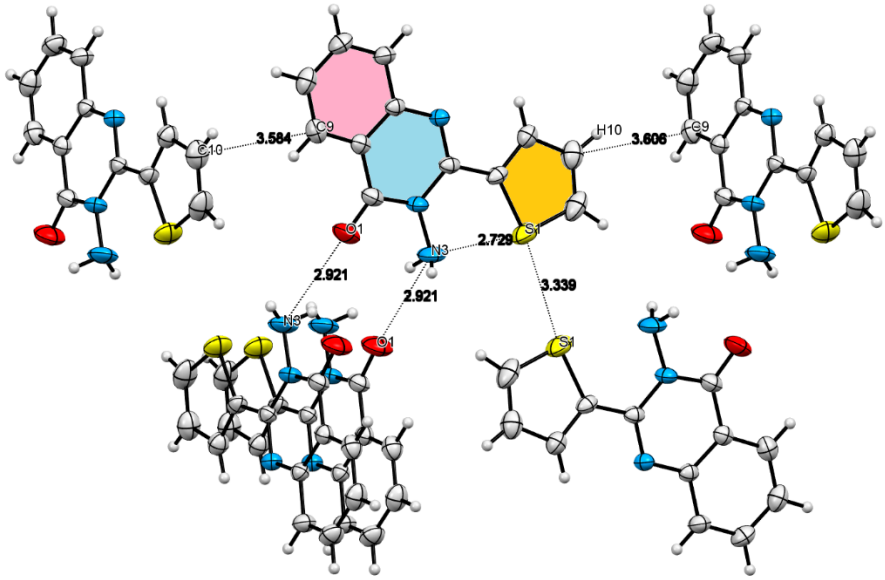

Fig.5. View showing the connection between the molecules by hydrogen bonds and π-stacking interactions (dashed lines**).**

The hydrogen bond π- π stacking interactions between neighbouring molecules make isolated fragments alternate along the b axis and leave them oriented along the c axis (**Fig.6**).

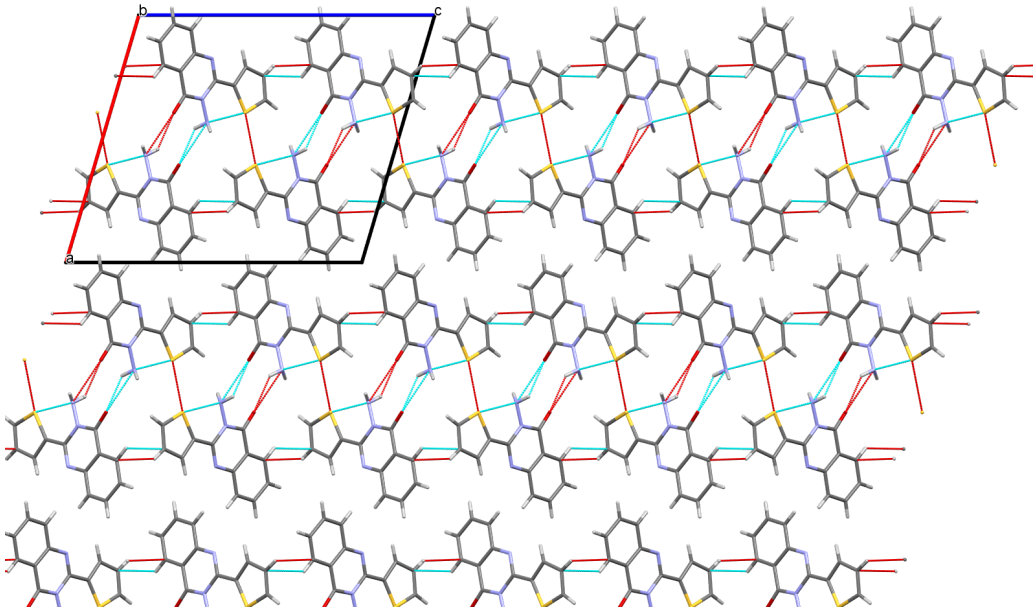

Fig.6. View of crystal packing of molecules: b- Projection

Computational details

The behaviour of the intermolecular interactions in the crystal was investigated using Hirshfeld surface analysis. CrystalExplorer [47] allowed us to generate a Hirshfeld surface of the title compound. Analysing the intermolecular contacts around the asymmetric unit using Hirshfeld surface d_{norm} mapping revealed

different intermolecular interactions (**Fig. 7**). In the relevant connections on the Hirshfeld surface, the red spots represent the shorter hydrogen bond interactions: S…S (3.092 Å), CH···CH (2.321 Å and 2.116 Å) and C=O···NH_2 (3.639 Å and 2.735 Å). The red regions indicate the numerous hydrogen bonds on the d_{norm} surface, which correlate with the results obtained using X-ray diffraction.

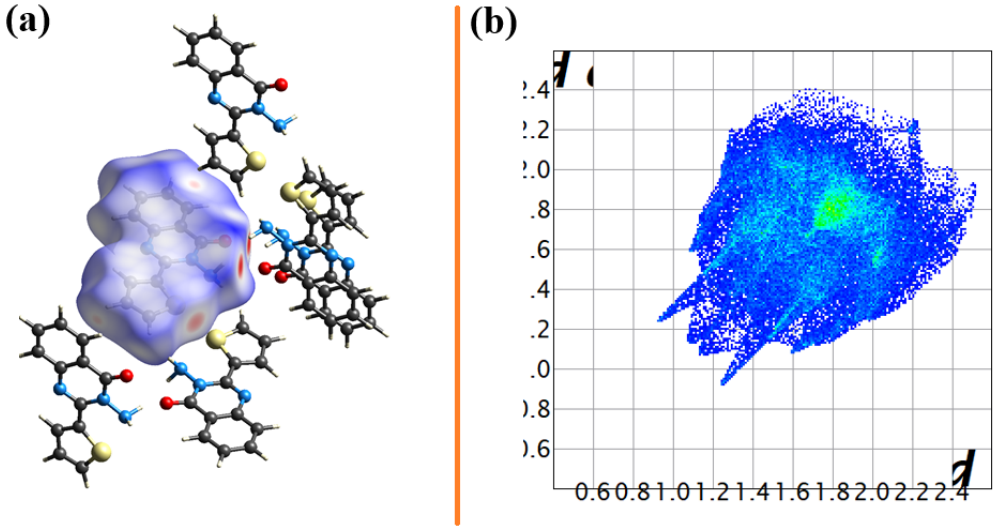

Fig.7. Hirshfeld surface mapped over d_{norm} (a) of the asymmetric unit and 2D fingerprint plot (b) for the title compound.

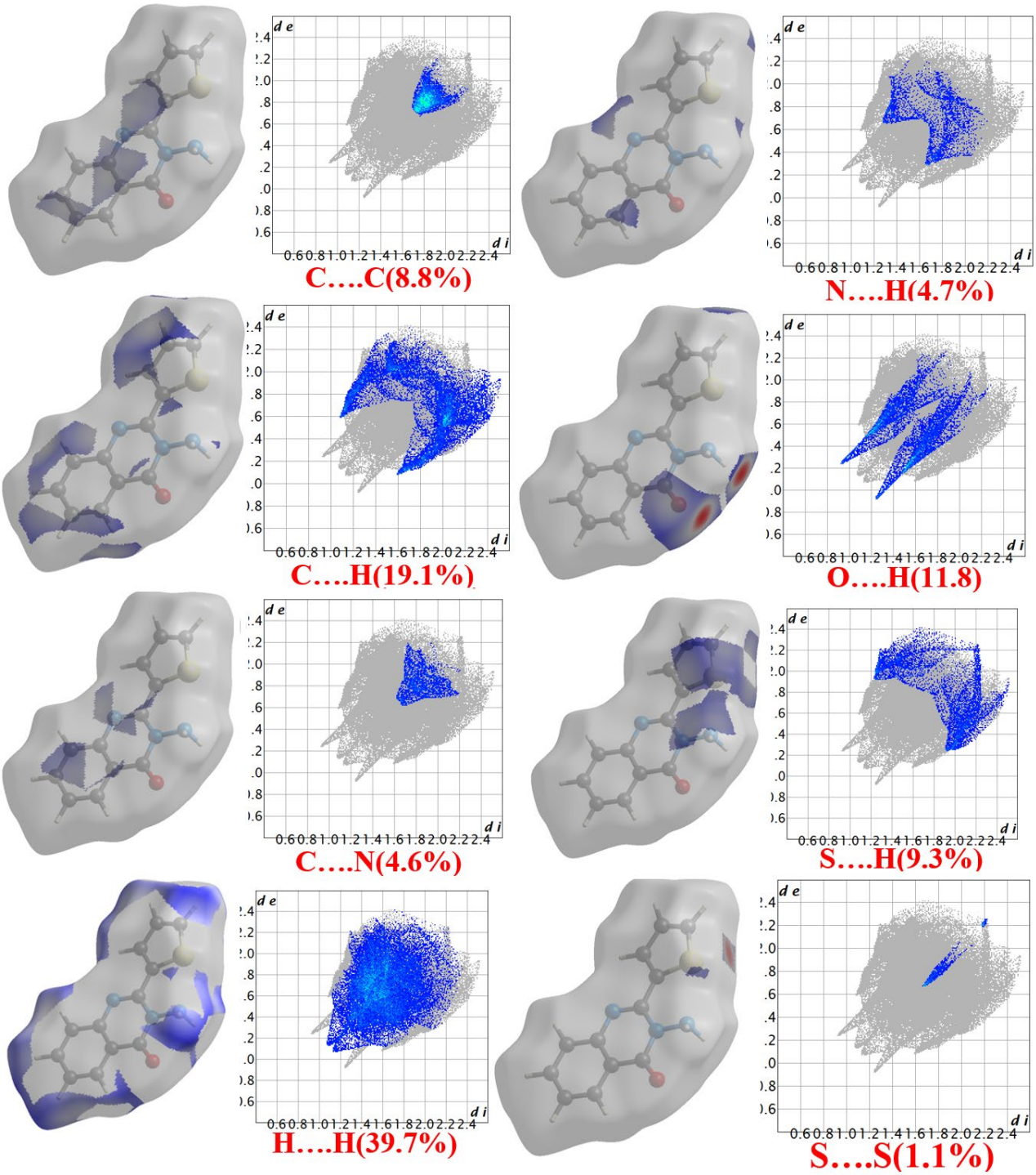

Fig.8. The two-dimensional fingerprint plots for the title compound showing the most intercontacts.

The intermolecular contacts within the $C_{12}H_9N_3OS$ and the ratios of their contributions were also identified (**Fig.8**). Overall, the H···O/O···H, H···H, H···C/C···H, S···H/H···S and N···H/H···N contacts were the most favourable (79.7%) in the crystal packing, while the H···N/N···S and N···C/C···N contacts represented 9.3% of the total Hirshfeld surface, making them the second-most-frequent interactions due to the abundance of hydrogen atoms on the molecular surface. The S···N/ N···S, S···S, S···N/ N···S, C···S/S···C and O···N/N···O contacts represented 2.8% of the total Hirshfeld surface. Quantitative analysis

showed that the C···H, H···H and H···O intermolecular hydrogen bonds were the most contacts, as they cooperate in building crystal packing.

Density functional theory (DFT) calculations at the B3LYP/6-311+ G(d,p) level of theory were performed using the Gaussian 16w package [48]. Visualization of the results was done using Gauss View 6.1.1 software [49]. The positively and negatively charged electrostatic potential of the $C_{12}H_9N_3OS$ was localised based on the calculated electrostatic surface potential (ESP; **Fig.9**). In **Figure 8**, the red area represents the electrostatic potential minimum, which is responsible for electrophilic attack. The blue colour represents the electrostatic potential maximum, which acts in the opposite manner. The pair of oxygen atoms in the acetamide forms a hydrogen-bond acceptor, which is consistent with the Hirshfeld surface analysis, indicating a strong intermolecular hydrogen bond with NH_2.

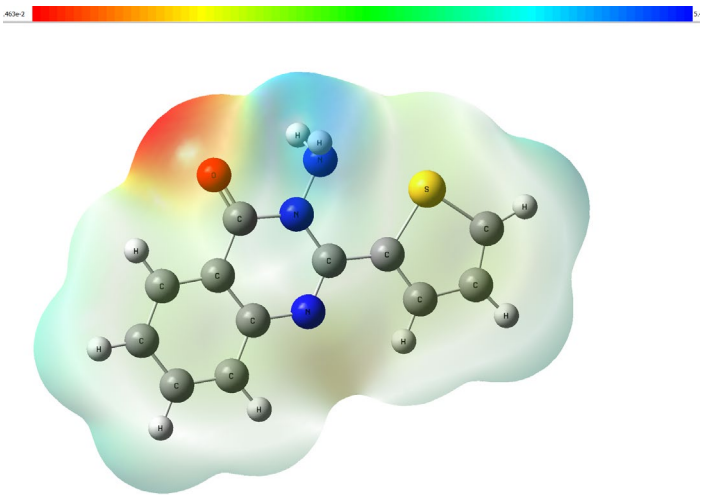

Fig.9. Electrostatic surface potential of $C_{12}H_9N_3OS$ obtained at the B3LYP/6-311 level of theory.

Figure 10 shows the optimised structure of the $C_{12}H_9N_3OS$. The bond lengths are in agreement, their deviations were between 0.008 Å–0.016 Å for the C-C bonds, 0.02 for the C=O Å bonds, 0.016 Å–0.03 Å for the C-N bonds and 0.096 Å–0.052 Å for the C-S bonds. The length of the C-C bonds varied between 1.348 Å and 1.464 Å, and the length of the N-N bonds was about 1.414 Å.

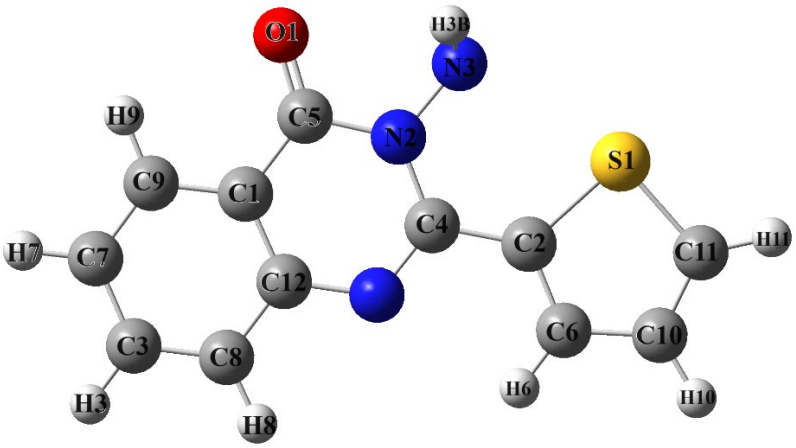

Fig.10. Optimized structure calculated by the DFT/B3LYP/6-311G method.

The length of the C=O bonds was about 1.230 Å, and the C-S bond length varied between 1.702 Å and 1.772 Å (**Table 2**). As seen, this deviation is not surprising given that theoretical calculation belongs to the isolated molecule and the experimental result belongs to the molecule in the solid state with intermolecular interactions and crystal packing effect. This clearly indicates that the calculation precision is satisfactory

Table 2. Experimental theoretical bond length comparison

Bond length (Å)	**experimental**	**Theoretical**
C-S	1.702 and 1.772	1.798 and 1.824
C-C	1.348, 1.414, 1.388, 1.467, 1.410, 1.372, 1398, 1.376, 1.399, 1.447, 1.402	1.364, 1.424, 1.375, 1.459, 1.409, 1.385, 1.410, 1.386, 1.406, 1.452, 1.418
N-N	1.414	1.414
C=O	1.23	1.25
C-N	1.385, 1.389, 1.299, 1.380	1.401, 1.419, 1.315, 1.398

Antimicrobial performance of derivative 4

Once synthesised, the antibacterial efficacy of product **4** was evaluated against different pathogens, including the gram-positive bacterial strains methicillin-resistant Staphylococcus aureus (MRSA) and Bacillus cereus (Bc) and the gram-negative strains Klebsiella pneumoniae (Kp) and Escherichia coli (E. coli). The MICs (minimum inhibitory concentrations) of the tested compound against four strains of bacteria is depicted in **Table 3**.

Table 3. Antibacterial effects of derivative **4** on the pathogens tested

		Pathogens			
		Klebsiella pneumoniae	*Escherichia coli*	*Methicillin-resistant Staphylococcus aureus*	*Bacillus cereus*
Compound **4**	MIC (µg/ml)	9.5	9.5	25	9.5
	MBC (µg/ml)	12.5	12.5	18.75	12.5
	Inhibition zone in mm (100 µg/ml)	25	24	14	22

The minimum inhibitory concentration (MIC) of compound **4** against bacterial strains is indicated in **Table 3**. Klebsiella pneumoniae, Escherichia coli, and Bacillus cereus were found to be sensitive to the tested compound (**4**) with a MIC of 9.5 µg/mL. However, compound **4** showed less efficacy against the Methicillin-resistant Staphylococcus aureus strain, exhibiting a MIC value of 25 µg/mL. It is evident that the hybridization of the two starting products **1** and **2**, along with the introduction of the hydrazine moiety to enhance the probability of hydrogen bonding with the biological target, has resulted in antibacterial

activity against the four bacterial strains selected in this study. The comparison of the results obtained in this study with the literature, especially those found by Yu Deng and his team, appears less significant, perhaps due to the presence of a bulkier group on carbon C2 which increases the likelihood of hydrogen bonding interactions with the biological target (**Fig. 11**) [50]. In the same comparative context, another series of compounds from the same family was synthesized and tested against a set of bacterial strains, showing significant results compared to our compound tested in this study. The structural difference between our work and that of Daniel Francis and his collaborators lies in the fact that their synthesized series substituted aryl groups on nitrogen atom N1 (**Fig. 11**) [51]. The conclusion drawn from this bibliographic analysis is that antibacterial activity is directly linked to the nature of substitutions at positions N1 and C2. On our part, the presence of the -NH_2 group on N1 and the thiophene group on C1 appear to have a weak effect on the biological target.

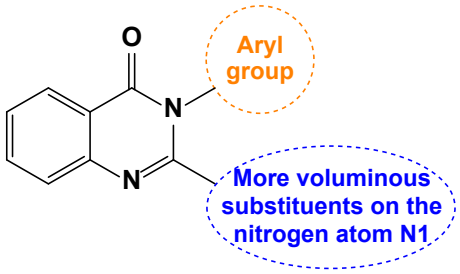

Fig. 11. Comparative analysis of the antibacterial activity of compound 4 with the literature.

Physico-chemical parameters

The physico-chemical parameters of the lead compound, as summarized in **Table 4**. Compound **4** exhibited a Log P value of 2.34, indicating moderate lipophilicity, which could influence its permeability and distribution within biological systems. The Total Polar Surface Area (TPSA) of 60.92 $Å^2$ suggests a moderate surface area available for interaction with biological targets, potentially impacting its binding affinity. With a molecular weight (MW) of 243.29 g/mol, compound **4** falls within the desirable range for drug-like molecules, balancing size and solubility considerations. The number of Hydrogen Bond Acceptors (HBA) and Donors (HBD) were found to be 3 and 1, respectively, indicating potential sites for intermolecular interactions crucial for ligand-receptor binding. Moreover, the compound possesses one rotatable bond, which could influence its conformational flexibility, impacting binding modes. Significantly, there were no violations observed, suggesting good adherence to Lipinski's rule of five, a guideline for predicting oral bioavailability of compounds. These physico-chemical parameters collectively contribute to understanding the drug-like properties of compound **4**, which are essential considerations in rational drug design and optimization strategies.

Table 4. Physico-chemical parameters of lead compound

Compound	Log P	TPSA	MW	HBA	HBD	No of Rotatable Bonds	No of Violations
4	2.34	60.92	243.29	3	1	1	0

Toxicity

The toxicity assessment of compound **4** presented in **Table 5.** The results demonstrated active towards hepatotoxicity and carcinogenicity, with probabilities of 0.60 and 0.61, respectively. However, it exhibited inactivity in terms of immunotoxicity, mutagenicity, and cytotoxicity, with probabilities of 0.99, 0.52 and 0.88, respectively, suggesting lower risks in these areas. These findings highlighting its relative safety in terms of immunotoxic, mutagenic, and cytotoxic effects.

Table 5. Toxicity score

Co*	Hepatotoxicity		Carcinogenicity		Immunotoxicity		Mutagenicity		Cytotoxicity	
	Toxicity	Prob	Toxicity	Prob	Toxicity	Prob	Toxicity	Prob	Toxicity	Prob
4	active	0.60	Active	0.61	Inactive	0.99	Inactive	0.52	Inactive	0.88

Co*: Compound

Molecular docking

The molecular docking results shown in **Table 6** and revealed significant binding affinities of Compound 4 with Klebsiella pneumoniae (PDB ID: 5O7N), E.Coli (PDB ID: 2JVU), Methicillin-resistant Staphylococcus aureus (PDB ID: 2W9S), and Bacillus cereus (PDB ID: 2HUC), with binding scores of -7.01, -5.76, -5.06 and -6.76 Kcal/mol, respectively. These scores indicate strong interactions between compound **4** and the target bacterial proteins. In Klebsiella pneumoniae, compound **4** formed hydrogen bonds with ILE 80 and THR 78 residues, along with a Pi Alkyl interaction with PRO 81 and a Pi Cation interaction with LYS 77. Similarly, in E.Coli, it engaged in hydrogen bonding with ASP 73 and ASN 46, Pi-Alkyl interactions with ALA 47 and ILE 78, and a Pi-Sigma interaction with THR 165. Methicillin-resistant Staphylococcus aureus showed hydrogen bonding with VAL 41 and SER 37, Pi-Alkyl with VAL 66, and a Sulfur-X interaction with PRO 40. Lastly, Bacillus cereus exhibited hydrogen bonding with ALA 7 and ILE 47, Pi-Sigma with LEU 20 and THR 46, and a Pi-Pi T shaped interaction with PHE 92. These diverse interaction patterns are shown in **Figure 12** and indicating the versatility of Compound 4 in recognizing and binding to different bacterial strains through a combination of hydrogen bonds, pi interactions, alkyl interactions, and cation-pi interactions. Comparatively, the standard drugs demonstrated binding scores of -4.37 kcal/mol for Meropenem, -6.82 kcal/mol for Ciprofloxacin, 0.36 kcal/mol for Vancomycin and -5.35 kcal/mol for Ampicillin. These results indicate that compound **4** exhibits superior binding affinities against these bacterial strains compared to standard drugs.

Table 6. Molecular docking results of compound **4** with various antibacterial targets

Target	Klebsiella pneumoniae	E.Coli	Methicillin-resistant Staphylococcus aureus	Bacillus cereus
PDB ID	5O7N	2JVU	2W9S	2HUC
Compound number	Binding Score In K.Cal/mol	Binding Score In K.Cal/mol	Binding Score In K.Cal/mol	Binding Score In K.Cal/mol
4	-7.01	-5.76	-5.06	-6.76
Standard	Meropenem -4.37	Ciprofloxacin -6.82	Vancomycin 0.36	Ampicillin -5.35
Type of Interactions with amino acid	ILE 80, THR 78 Hydrogen Bond PRO81 Pi Alkyl LYS77 Pi Cation	ASP73, ASN 46 Hydrogen Bond ALA47, ILE 78 Pi-Alkyl THR165PiSigma	VAL 41, SER37 Hydrogen Bond VAL 66 Pi-Alkyl PRO 40 Sulfur-X	ALA 7, ILE 47 Hydrogen Bond LEU 20, THR 46 Pi-Sigma PHE 92 Pi-Pi T shaped

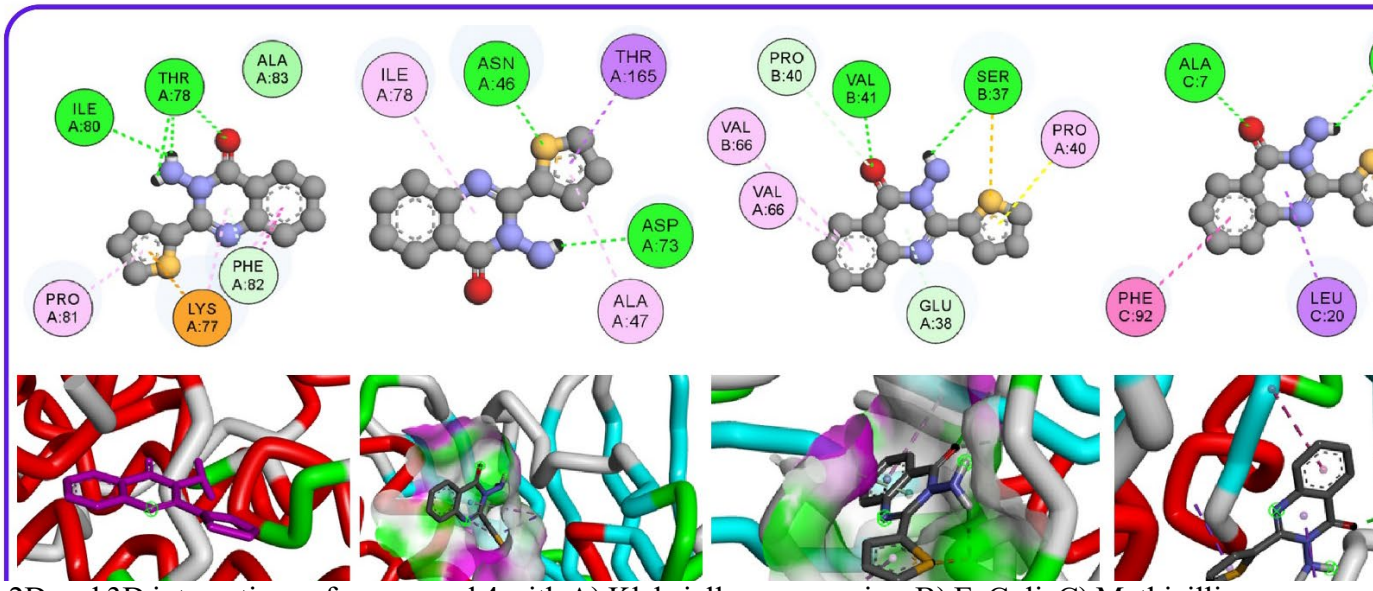

Fig.12. 2D and 3D interactions of compound **4** with A) Klebsiella pneumoniae, B) E. Coli, C) Methicillin-resistant Staphylococcus aureus, and D) Bacillus cereus.

Conclusion

A novel 3-amino-2-(2-thienyl)-4(3H)-quinazolinone derivative was produced from anthranilic acid using a novel two-step chemical process based on 2-thiophenecarboxaldehyde and hydrazine. The heterocyclic system has been fully identified using spectroscopic and crystallographic data. The compound crystallised in a monoclinic system within the P21/c space group. The hydrogen bonds and weak π-π stacking interactions assured the cohesion between molecules, which allowed the crystal to be constructed. The contributions of these interactions were analysed using a Hirshfeld surface. In addition, the electrostatic surface potential was determined using the DFT method to locate the positively and negatively charged electrostatic potential in the molecule. The quinazoline derivative synthesised was applied to selected bacterial pathogens, and its antibacterial activity was evaluated. The results showed that the derivative exerted activity against all bacterial pathogens tested. The experimental results of this antibacterial test have been confirmed by a molecular docking study.

References

[1] D. Geetika, S. Paramita, S. Sandip, H. Jayanta, Battle against vancomycin resistant bacteria: recent developments in chemical strategies, J. Med. Chem. 62 (2019) 3184-3205.
[2] O. Sultan, K. Muhammet, K. Ferudun, T. Ferhan, Synthesis, characterization, and antibacterial effect of diarylmethylamine-based imines, J. Mol. Struct. 1214 (2020) 128150.
[3] M.N. Alekshun, S.B. Levy, Molecular mechanisms of antibacterial multidrug resistance, Cell. 128 (2007) 1037-1050.
[4] A. Parmanik, S. Das, B. Kar, A. Bose, G.R. Dwivedi, M.M. Pandey, Current treatment strategies against multidrug-resistant bacteria: a review, Curr. Microbil. 79 (2022) 388.
[5] A. Catalano, D. Iacopetta, J. Ceramella, D. Scumaci, F. Giuzio, C. Saturnino, S. Aquaro, C. Rosano, M.S. Sinicropi, Multidrug Resistance (MDR): a widespread phenomenon in pharmacological therapies, Molecules. 27 (2022) 616.
[6] Y. Qin, M. Sun, N. Zhang, Y. Yang, P. Ma, Synthesis and biological evaluation of antibacterial activity of novel clarithromycin derivatives incorporating 1,2,3-triazole moieties at the 4- and 11- OH positions, Bioorg. Chem. 127 (2022) 106020.
[7] K.C. Nicolaou, S. Jason, D.J. Chen, Recent Advances in the Chemistry and Biology of Naturally Occurring Antibiotics, Angew. Chem. Int. Ed. Engl. 48 (2009) 660-719.
[8] Z.Z. Ma, Y. Hano, T. Nomura, Y.J. Two. New pyrroloquinazolinoquinoline alkaloids from Peganum nigellastrumChen, Heterocycles. 46 (1997) 541.
[9] Z. Somayeh, E. Leila, F. Zahra, Z. Farshid, F. Zeinab, K. Soghra, Design, synthesis, computational study and cytotoxic evaluation of some new quinazoline derivatives containing pyrimidine moiety. Scien. Rep. 13 (2023) 14461
[10] C. Wattanapiromsakul, P.I. Forster, P.G. Waterman, Alkaloids and limonoids from Bouchardatia neurococca: systematic significance, Phytochemistry. 64 (2003) 609
[11] B. Moy, P. Kirkpatrick, S. Kar, P. Goss, Lapatinib, Nat. Rev. Drug Discov. 6 (2007) 431
[12] A.A. Farag, E.M. Khalifa, N.A. Sadik, S.Y, Abbas. Synthesis, characterization, and evaluation of some novel 4 (3 H)-quinazolinone derivatives as anti-inflammatory and analgesic agents. Med. Chem. Res. 22 (2013) 440-452.
[13] S. Gatadi, T.V. Lakshmi, S. Nanduri. 4(3H)-Quinazolinone derivatives: Promising antibacterial drug leads, Eur. J. Med. Chem. 15 (2019) 157-172.
[14] A. Hatem, H. Ahmed, H. Mohamed, H. Rashid, A.E. Gamal, R. Al-Salahi. Benzo[g]quinazolines as antifungal against candidiasis: Screening, molecular docking, and QSAR investigations, Saudi Pharm. J. 31 (2023) 815-823.
[15] A. Dutta, D. Sarma. Recent advances in the synthesis of Quinazoline analogues as Anti-TB agents. Tuberculosis. 124 (2020) 101986.
[16] V. Alagarsamy, Raja. S.V, M.Murugan, K.Dhanabal, P. Parthiban. Design and synthesis of 3-(4-ethylphenyl)-2-substituted amino-3 H-quinazolin-4-ones as a novel class of analgesic and anti-inflammatory agents, J. Enzy. Inhib. Medi. Chem, 23 (2008) 839-847.
[17] R. Lakhan, O.P. Singh, R.L. Singh-J. Studies on 4 (3H)-quinazolinone derivatives as anti-malarials, J. Indian. Chem. Soc. 64 (1987) 316-318.
[18] M.S. Malamas, J. Millen. Quinazolineacetic acids and related analogs as aldose reductase inhibitors, J. Med. Chem. 34 (1991) 1492-1503.
[19] M. Alvarado, M. Barceló, L. Carro, C.F. Masaguer, E. Raviña, Synthesis and biological evaluation of new quinazoline and cinnoline derivatives as potential atypical antipsychotics, Chem. Biodivers. 3 (2006) 106-117.
[20] E. Ataollahi, M. Behrouz, P. Mardaneh, M. Emami, H. Zafarian, S. Khabnadideh, L. Emami, Novel quinazolinone derivatives as anticancer agents: Design, synthesis, biological evaluation and computational studies, J. Mole. Stru. 1295 (2024) 136622.
[21] S. Zare, L. Emami, Z. Faghih, F. Zargari, Z. Faghih, S. Khabnadideh, Design, synthesis, computational study and cytotoxic evaluation of some new quinazoline derivatives containing pyrimidine moiety, Sci. Rep. 13 (2023) 14461.

[22] X. Chen, H. Wei, L. Yin, X. Li, A. convenient synthesis of quinazoline derivatives via cascade imimo-Diels-Alder and oxidation reaction, Chin. Chem. Lett. 21 (2010) 782-786.
[23] P. He, Y.B. Nie, J. Wu, M.W. Ding, Unexpected synthesis of indolo[1,2-c]quinazolines by a sequential ugi 4CC-Staudinger-aza-Wittig-nucleophilic addition reaction, Org. Biomol. Chem. 9 (2011) 1429-1436.
[24] H. Luo, D. Hu, J. Wu, M. He, L. Jin, S. Yang, B. Song, Rapid synthesis and antiviral activity of (quinazolin-4-ylamino)methyl-phosphonates through microwave irradiation, Int. J. Mol. Sci. 13 (2012) 6730-6746.
[25] G. Qiu, Y. He, J. Wu, Preparation of quinazolino[3,2-a]quinazolines via a palladium-catalyzed three-component reaction of carbodiimide, isocyanide, and amine, Chem. Commun. 48 (2012) 3836-3838.
[26] M.A. McGowan, C.Z. McAvoy, S.L. Buchwald, Palladium-catalyzed N-monoarylation of amidines and a one-pot synthesis of quinazoline derivatives, Org. Lett. 14 (2012) 3800-3803.
[27] P. Sang, Y.J. Xie, J.W. Zou, Y.H. Zhang, Copper-catalyzed sequential Ullmann N-arylation and aerobic oxidative C-H amination: a convenient route to indolo[1,2-c]quinazoline derivatives. Org Lett. 14 (2012) 3894-3897.
[28] A.K. Khalil, Phase-transfer catalyzed alkylation and cycloalkylation of 2-mercaptoquinazolin-4(3H)-one, Phosphorus. Sulfur. 180 (2005) 2533-2541.
[29] V.N. Emiliya, N.L. Galina, V.P. Yulia, N.C. Valery, Quinazolines annelated at the N(3)–C(4) bond: Synthesis and biological activity, Euro. J. Med. Chem. 271 (2024) 116411
[30] R. Rohini, K Shanker, P.M. Reddy, Y.P. Ho, V. Ravinder, Mono and bis-6-arylbenzimidazo[1,2-c]quinazolines: A new class of antimicrobial agents, Eur. J. Med. Chem. 44 (2009) 3330-3339.
[31] S. Tu, C. Li, G. Li, L. Cao, Q. Shao, D. Zhou, B. Jiang, J. Zhou, M. Xia. Microwave-assisted combinatorial synthesis of polysubstituent imidazo[1,2-a]quinoline, pyrimido[1,2-a]quinoline and quinolino[1,2-a]quinazoline derivatives, J. Comb. Chem. 9 (2007) 1144-1148.
[32] O.A. Olayinnka, Y.A. Oluwatosin, W.G. Markus, L.B. Babatunde, Expeditious Synthesis and Spectroscopic Characterization of 2-Methyl-3-substituted-quinazolin-4(3H)-one Derivatives. Orient. J. Chem. 33 (2017) 562-574.
[33] A. Altomare, M.C. Burla, M. Camalli, G.L. Cascarano, C. Giacovazzo, A. Guagliardi, A.G. Moliterni, G. Polidori, R.J.J.o.A.C. Spagna, SIR97: a new tool for crystal structure determination and refinement, J. App. Cryst. 32 (1999) 115-119.
[34] G. Sheldrick, SHELXL-97 (Release 97-2) University of Göttingen, Germany, 1998.
[35] C.F. Macrae, I.J. Bruno, J.A. Chisholm, P.R. Edgington, P. McCabe, E. Pidcock, L. Rodriguez-Monge, R. Taylor, J. Streek, P.A. Wood, Mercury CSD 2.0–new features for the visualization and investigation of crystal structures, J. Appl. Crystall. 41 (2008) 466-470.
[36] Farrugia, L.J. WinGX suite for small-molecule single-crystal crystallography. J. Appl. Cryst. 1999, 32, 837–838.
[37] M.A. Spackman, D. Jayatilaka, Hirshfeld surface analysis, Cryst. Eng. Comm. 11 (2009) 19-32.
[38] J.J. McKinnon, D. Jayatilaka, M.A. Spackman, Towards quantitative analysis of intermolecular interactions with Hirshfeld surfaces, Chem. Commun. (2007) 3814-3816.
[39] R.S. Peter, J.T. Michael, J.M. Joshua, K.W. Stephen, J.G. Daniel, J. Dylan, A.S. Mark, CrystalExplorer: a program for Hirshfeld surface analysis, visualization and quantitative analysis of molecular crystals. J. Appl. Crystallogr. 54 (2021) 1006-1011
[40] Gaussian 16, Revision C.01, M. J. Frisch, G. W. Trucks, H. B. Schlegel, G. E. Scuseria, M. A. Robb, J. R. Cheeseman, G. Scalmani, V. Barone, G. A. Petersson, H. Nakatsuji, X. Li, M. Caricato, A. V. Marenich, J. Bloino, B. G. Janesko, R. Gomperts, B. Mennucci, H. P. Hratchian, J. V. Ortiz, A. F. Izmaylov, J. L. Sonnenberg, D. Williams-Young, F. Ding, F. Lipparini, F. Egidi, J. Goings, B. Peng, A. Petrone, T. Henderson, D. Ranasinghe, V. G. Zakrzewski, J. Gao, N. Rega, G. Zheng, W. Liang, M. Hada, M. Ehara, K. Toyota, R. Fukuda, J. Hasegawa, M. Ishida, T. Nakajima, Y. Honda, O. Kitao, H. Nakai, T. Vreven, K. Throssell, J. A. Montgomery, Jr., J. E. Peralta, F. Ogliaro, M. J. Bearpark, J. J. Heyd, E. N. Brothers, K. N. Kudin, V. N. Staroverov, T. A. Keith, R. Kobayashi, J. Normand, K. Raghavachari, A. P. Rendell, J. C. Burant, S. S. Iyengar, J. Tomasi, M. Cossi, J. M. Millam, M. Klene, C. Adamo, R. Cammi, J. W. Ochterski, R. L. Martin, K. Morokuma, O. Farkas, J. B. Foresman, and D. J. Fox, Gaussian, Inc., Wallingford CT, 2019.

[41] J. Tomasi, B. Mennucci, E. Cancès, The IEF version of the PCM solvation method: an overview of a new method addressed to study molecular solutesat the QM ab initio level, J. Mol. Struct: Theochem. 464 (1999) 211-226.
[42] Molinspiration Cheminformatics free web services, Slovensky Grob, Slovakia. https://www.molinspiration.com https://www.molinspiration.com.
[43] C.A. Lipinski, F. Lombardo, B.W. Dominy, P.J. Feeney, Experimental and computational approaches to estimate solubility and permeability in drug discovery and development settings, Adv. Drug. Delivery. Rev. 23 (1997) 4-25.
[44] P. Banerjee, A.O. Eckert, A.K. Schrey, R. Preissner, ProTox-II: a webserver for the prediction of toxicity of chemicals, Nucleic Acids Res. 46 (2018) 257-263.
[45] N.R. Babu, B.M. Sahoo, T. Radhika, Synthesis, Antitubercular Evaluation, Molecular Docking Study, and Teratogenicity Studies of Novel Triazolo Quinazoline Hybrids, Russ. J. Gen. Chem. 93 (2023) 2684-2693.
[46] C. Janiak, A critical account on π–π stacking in metal complexes with aromatic nitrogen-containing ligands, J. Chem. Soc., Dalton Trans. 21 (2000) 3885-3896.
[47] M. Turner, J. McKinnon, P. Grimwood, M. Spackman, CrystalExplorer. Version 17. University of Western Australia, 2017.
[48] M. Frisch, G. Trucks, H. Schlegel, G. Scuseria, M. Robb, J. Cheeseman, G. Scalmani, V. Barone, G. Petersson, H. Nakatsuji, Gaussian 16, revision C. 01. Wallingford: Gaussian, Inc, 2016.
[49] T.K. Roy Dennington, and John Millam, GaussView, Version 6.1.1, , Semichem Inc., Shawnee Mission, KS, 2019.
[50] F. Daniel, F. Sannia, M. Archie, D. Didi, L. Abbie, W. Stuart, J.N. Alex, Algorithm-driven activity-directed expansion of a series of antibacterial quinazolinon, Org. Biomol. Chem. 20 (2022) 9672-9678
[51] D. Yu, Z. Yang, C. Xiao-Hu, L. Cheng-Hong, Antibacterial activity evaluation of pleuromutilin derivatives with 4(3H)-quinazolinone scaffold against methicillin-resistant Staphylococcus aureus, Eu. J. Med. Chem. 246 (2023) 114960